Korean J. Chem. Eng., 32(11), 2212-2219 (2015)
DOI: 10.1007/s11814-015-0062-6

pISSN: 0256-1115
eISSN: 1975-7220

Propane combustion over Pt/Al_2O_3 catalysts with different crystalline structures of alumina

Jung Eun Park, Bo Bae Kim, and Eun Duck Park†

Department of Chemical Engineering and Department of Energy Systems Research, Ajou University, 206, Worldcup-ro, Yeongtong-gu, Suwon 443-749, Korea
(*Received 19 October 2014 • accepted 1 April 2015*)

Abstract−The effects of the crystalline phases (α-Al_2O_3, κ-Al_2O_3, δ-Al_2O_3, θ-Al_2O_3, η-Al_2O_3, and γ-Al_2O_3) of the alumina support of Pt/Al_2O_3 catalysts on the catalyst activity toward propane combustion were examined. The catalysts were characterized by N_2 physisorption, CO chemisorption, temperature-programmed reduction (TPR), temperature-programmed oxidation (TPO), transmission electron microscopy (TEM), and infrared spectroscopy (IR) after CO chemisorption. The Pt dispersion of the catalysts (surface Pt atoms/total Pt atoms), measured via CO chemisorption, was more dependent on the crystalline structure of alumina than on the surface area of alumina. The highest catalytic activity for propane combustion was achieved with Pt/α-Al_2O_3, which has the lowest Brunauer, Emmett, and Teller (BET) surface area and Pt dispersion. The lowest catalytic activity for propane combustion was exhibited by Pt/γ-Al_2O_3, which has the highest BET surface area and Pt dispersion. The catalytic activity was confirmed to increase with increasing Pt particle size in Pt/δ-Al_2O_3. The apparent activation energies for propane combustion over Pt/α-Al_2O_3, Pt/κ-Al_2O_3, Pt/δ-Al_2O_3, Pt/θ-Al_2O_3, Pt/η-Al_2O_3, and Pt/γ-Al_2O_3 were determined to be 24.7, 21.4, 24.3, 22.1, 24.0, and 19.1 kcal/mol, respectively.

Keywords: Propane Combustion, Pt, Alumina, Support, Oxidation

INTRODUCTION

Propane is one of the major components of the widely utilized fuel, liquefied petroleum gas (LPG), which finds a variety of applications owing to its high energy density, clean combustion, and easy storage and delivery through a well-established infrastructure. Propane is also considered to be a model compound of the volatile organic compounds emitted from various sources, including transportation vehicles, during a cold start. Therefore, the catalytic combustion of propane has been investigated for power plant and emission-control applications [1].

Several noble metal-based catalysts have been investigated for application to low-temperature catalytic complete oxidation, which is an advantageous technique for energy conservation [1-6]. Pt-based catalysts have been reported to be superior compared to Pd- and Rh-based catalysts for low-temperature propane combustion [5,6].

To enhance the performance of Pt-based catalysts for low-temperature propane combustion, several factors that affect the catalytic performance have been examined, including the effects of different supports such as Al_2O_3, SiO_2, SiO_2-Al_2O_3, ZrO_2, yttria-stabilized zirconia, SO_4^{2-}-ZrO_2, CeO_2, MgO, La_2O_3, TiO_2, and zeolites [7-17]. The physicochemical properties of the support reportedly affect the particle size of Pt and the oxidation state of the Pt species, thereby impacting the catalytic activity for propane combustion. Park et al. reported that the dispersion of Pt in Pt catalysts supported on metal oxides increased with increasing surface area of the support for the same metal oxide, and that Pt catalysts on supports with lower surface areas (ZrO_2, CeO_2, and TiO_2) exhibited higher catalytic activity for propane combustion than Pt catalysts on supports with higher surface areas [9]. Hattori's group asserted that propane combustion over Pt-based catalysts was structure-sensitive and the turnover frequency (TOF) increased with increasing acid strength of the support because electrophilic support materials exhibited higher oxidation resistance than the electrophobic congeners [7,8]. On the other hand, Hubbard et al. reported that the acid strength of the support was not the major factor that influences propane combustion [11]. Burch et al. also reported that the catalytic activity of a fluorine-modified alumina-supported Pt catalyst was not higher than that of the Pt catalyst supported on sulfur dioxide-modified alumina, even though the acid strength of the former support is higher than that of the latter [12].

In addition to the supports, various metal (K, Mg, Al, Ce, V, W, Mo, and Zr) oxides have been examined as promoters for this reaction [6,17-23]. Hattori's group observed that the catalytic activity of the platinum catalyst varied drastically based on the types of additives present, and increased with increasing electronegativity of the additives. They concluded that the variation in the catalytic activity was derived from the variation in the oxidation state, and that the additives affected the catalytic activity by influencing the oxidation state of platinum [17,18].

Alumina has frequently been used as a catalyst support. Although alumina exists in several crystalline phases [24,25], the γ-Al_2O_3 support has primarily been used for low-temperature propane com-

†To whom correspondence should be addressed.
E-mail: edpark@ajou.ac.kr

bustion. The physicochemical properties of alumina are dependent on the crystalline phase; thus, the structural and electronic states of metal and metal oxides in supported metal and metal oxides might be altered by the support, resulting in the variation of the catalytic activity. In this study, the effects of various alumina crystalline phases on the performance of Pt/Al_2O_3 catalysts in propane combustion are examined. To exclude the adverse effect of residual chloride on the catalytic activity [26], $Pt(NO_3)_4(NO_3)_2$ is utilized as a Pt precursor in the preparation of the supported Pt catalysts.

EXPERIMENTAL

1. Catalyst Preparation

Various single-phase aluminum oxides (η-Al_2O_3, θ-Al_2O_3, δ-Al_2O_3, and κ-Al_2O_3) were prepared via the thermal decomposition of bayerite at 873 and 1,273 K, boehmite at 1,173 K, and gibbsite at 1,273 K [24]. α-Al_2O_3 (Kanto Chem.) and γ-Al_2O_3 (Alfa Aesar) were purchased and utilized as received for the support. All catalysts were prepared by an incipient wetness method using a support and an aqueous solution of $Pt(NH_3)_4(NO_3)_2$ (Sigma-Aldrich). The impregnated catalysts were dried overnight in an oven at 393 K, calcined in air at 773 K for 4 h, and finally reduced with H_2 at 673 K for 1 h prior to the reaction.

2. Catalyst Characterization

The surface area of each sample was measured by the Brunauer, Emmett, and Teller (BET) method based on the N_2 adsorption data obtained at 77 K using a Quantachrome Autosorb-1 instrument. Before the measurements, the samples were degassed under vacuum for 4 h at 473 K. The powder X-ray diffraction (XRD) patterns of the samples were obtained using a Rigaku D/MAC-III diffractometer with Cu Kα radiation (λ=1.5406 Å) operated at 40 kV and 100 mA. The Pt content of the prepared samples was analyzed by inductively coupled plasma-atomic emission spectroscopy (ICP-AES, JY-710 Plus, Jobin-Yvon).

The temperature-programmed reduction (TPR) and temperature-programmed oxidation (TPO) of the samples were conducted using an AutoChem 2,910 unit (Micromeritics) equipped with a thermal conductivity detector (TCD) to measure the H_2 consumption. A water trap composed of blue silica gel was used to remove moisture from the TPR effluent stream at 273 K before it reached the TCD. In general, a quartz U-tube reactor was loaded with 0.20 g of the sample. TPR was performed using 10 vol% H_2/Ar at a flow rate of 30 mL/min in the temperature range 203-1,173 K. All catalysts were calcined in air at 773 K for 4 h before the TPR experiments were conducted. Separately, TPO was performed using 2 vol% O_2/He at a flow rate of 30 mL/min in the temperature range 300-1,173 K at a heating rate of 10 K/min. All catalysts were reduced in 10 vol% H_2/Ar at 673 K for 1 h before the TPO experiments were conducted. The TCD signals were monitored after all the residual hydrogen was removed from the line by purging with He at 313 K for 1 h.

The pulsed CO chemisorption experiments were conducted using an AutoChem 2,910 unit (Micromeritics) equipped with a TCD to measure the CO consumption. In general, a quartz U-tube reactor was loaded with 0.20 g of the sample. All catalysts were reduced in H_2 at 673 K for 1 h and then cooled to room temperature. Chemisorption was carried out at 300 K under a 30 mL/min stream of He using a pulsed-chemisorption technique, where 500-μL pulses of CO were used. Based on the CO chemisorption data, the Pt dispersion (D) for each catalyst was calculated based on the assumption that one CO molecule is adsorbed per surface Pt atom. The average particle size of Pt (d) for each catalyst was also calculated from the Pt dispersion by using the following equation:

$$d(\text{Å}) = 6\frac{v_m/a_m}{D} \quad (1)$$

where v_m is the volume occupied by an atom in bulk metal (w_m= 15.10 $Å^3$ for Pt), D is the Pt dispersion, and a_m is the area occupied by a surface atom and calculated by using the following proportions of low index planes: (111) : (100) : (110)=1 : 1 : 1 (a_m=8.07 $Å^2$ for Pt) [27].

The particle size of Pt was estimated using transmission electron microscopy (TEM) images obtained on a JEM-2100F (JEOL) microscope operated at an acceleration voltage of 200 kV.

The infrared (IR) spectra after CO adsorption on the Pt/Al_2O_3 catalysts were recorded with a Nicolet 6700 spectrometer equipped with a mercury cadmium telluride (MCT) detector with 32 scans at an effective resolution of 4 cm^{-1} using an in situ IR cell with a CaF_2 window. Prior to each experiment, a self-supporting (13-mm diameter, 0.02 g) wafer was placed into the IR cell with the CaF_2 window connected to the vacuum system and reduced with H_2 at 573 K for 1 h. The background spectra of the sample were recorded after the self-supported wafer was cooled to room temperature and degassed under a pressure of 10^{-3} bar. The IR spectra were also acquired after adsorption of CO at room temperature for 0.5 h, purging with a He stream for 0.5 h, and degassing under a pressure of 10^{-3} bar.

3. Catalytic Activity Test

The propane combustion activities of the samples were measured at atmospheric pressure in a continuous fixed bed reactor containing 0.10 g of catalyst. All catalysts were reduced at 673 K for 1 h under a H_2 stream at a flow rate of 30 mL/min prior to the reaction. The catalyst was brought into contact with the reactant gas composed of 1 mol% propane and 5 mol% O_2 balanced with He flowing at a rate of 100 mL/min. Separately, the kinetic data were also obtained under the differential reactor conditions, where the propane conversion was regulated to be lower than 20% by adjusting the catalyst loading. To investigate the thermal stability of the Pt/α-Al_2O_3 and Pt/δ-Al_2O_3 catalysts, these catalysts were exposed to the reactant gas stream composed of 1 mol% propane and 5 mol% O_2 balanced with He at 773 K for 1 h, reduced in a H_2 stream at 673 K for 1 h, and evaluated for their catalytic activity. In all cases, the steady-state catalytic activities were measured at each temperature. The reactants and products were analyzed using a gas chromatograph (GC, HP 5890) equipped with a TCD and a flame ionization detector. The propane conversion was calculated by using the following formula:

$$C_3H_8 \text{ conversion } (\%) = \frac{[C_3H_8]_{in} - [C_3H_8]_{out}}{[C_3H_8]_{in}} \times 100 \quad (2)$$

A moisture trap was installed before the GC to remove the moisture formed during the reactions.

Table 1. Physicochemical properties of Pt catalysts supported on various aluminum oxides

Catalyst	Pt content[a] (%)	Surface area[b] (m^2/g)	Amount of chemisorbed CO[c] (μmol CO/$g_{cat.}$)	Dispersion, D[d]	Average Pt particle size, d[e] (nm)	Average Pt particle size, d[f] (nm)
Pt/α-Al_2O_3	1.00	<1	2.6	0.05	22	6.2±3.9
Pt/κ-Al_2O_3	0.95	22	17.5	0.36	3.1	4.2±0.2
Pt/δ-Al_2O_3	0.96	101	24.0	0.49	2.3	3.9±1.5
Pt/θ-Al_2O_3	0.91	80	15.6	0.30	3.7	4.3±0.8
Pt/η-Al_2O_3	0.95	219	14.1	0.29	3.9	4.5±1.3
Pt/γ-Al_2O_3	0.86	221	36.8	0.72	1.6	~1

[a]The Pt content was determined with ICP-AES
[b]The surface area was determined with the BET method based on the N_2 physisorption data
[c]CO chemisorptions were carried out at 300 K
[d]Dispersion (D) was calculated from the CO chemisorption data
[e]Average Pt particle size (d) was calculated from the Pt dispersion
[f]Average Pt particle size (d) was determined by counting Pt particles less than 10 nm with TEM images

RESULTS AND DISCUSSION

1. Physicochemical Properties of Catalysts

The N_2 physisorption data indicate that the supports did not contain micropores and that the pore volume decreased in the following order: δ-Al_2O_3>η-Al_2O_3>θ-Al_2O_3>γ-Al_2O_3>κ-Al_2O_3>α-Al_2O_3 [24]. The BET surface areas (Table 1) decreased in the following order: Pt/γ-Al_2O_3>Pt/η-Al_2O_3>Pt/δ-Al_2O_3>Pt/θ-Al_2O_3>Pt/κ-Al_2O_3>Pt/α-Al_2O_3.

The reducibility of the Pt species in the Pt/Al_2O_3 catalysts was compared with their TPR patterns, as shown in Fig. 1. For all catalysts, except Pt/α-Al_2O_3, two strong TPR peaks were observed at 460 and 630 K. The TPR peak position and its intensity are related to the reducibility and amount of reducible species on the catalyst, respectively. In general, the reduction of Pt/Al_2O_3 catalysts is characterized by two main peaks. The peak at lower temperature (<523 K) may be due to the bulk phase of the platinum species, including Pt_sO (surface platinum oxide), PtO, and PtO_2. The TPR peak below room temperature is associated with PtO interacting weakly with the support. The TPR peak at high temperatures (>523 K) may be due to the formation of an inorganic Pt complex with isolated platinum oxides. Hwang et al. reported that the TPR peak at high temperatures was related to a high stoichiometric value of the O/Pt ratio in the PtO_x complex or the formation of $PtAl_2O_4$ spinel species [28]. Therefore, it can be said that there are two different Pt species, one is weakly interacting with a support and the other is strongly binding to the support, in all Pt/Al_2O_3 catalysts, except

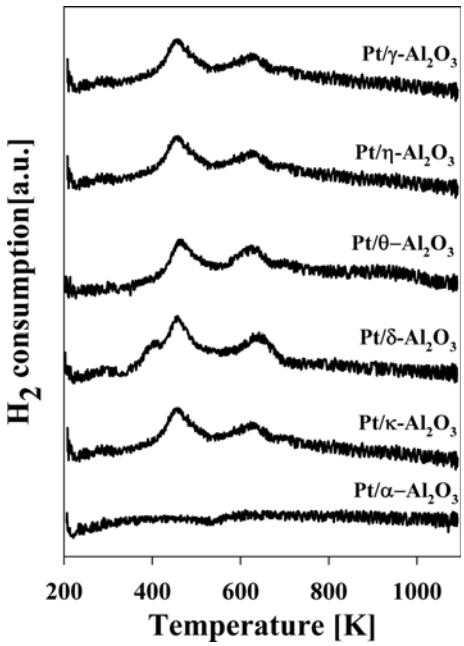

Fig. 1. Temperature-programmed reduction profiles of Pt catalysts supported on different aluminum oxides. All catalysts were calcined in air at 773 K prior to analysis.

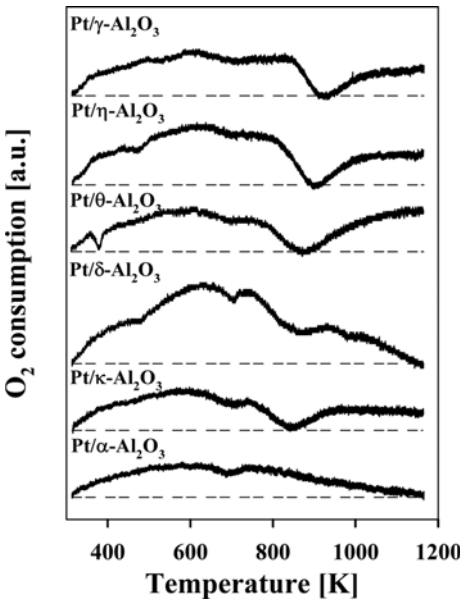

Fig. 2. Temperature-programmed oxidation profiles of Pt catalysts supported on different aluminum oxides. All catalysts were reduced with H_2 at 673 K prior to analysis.

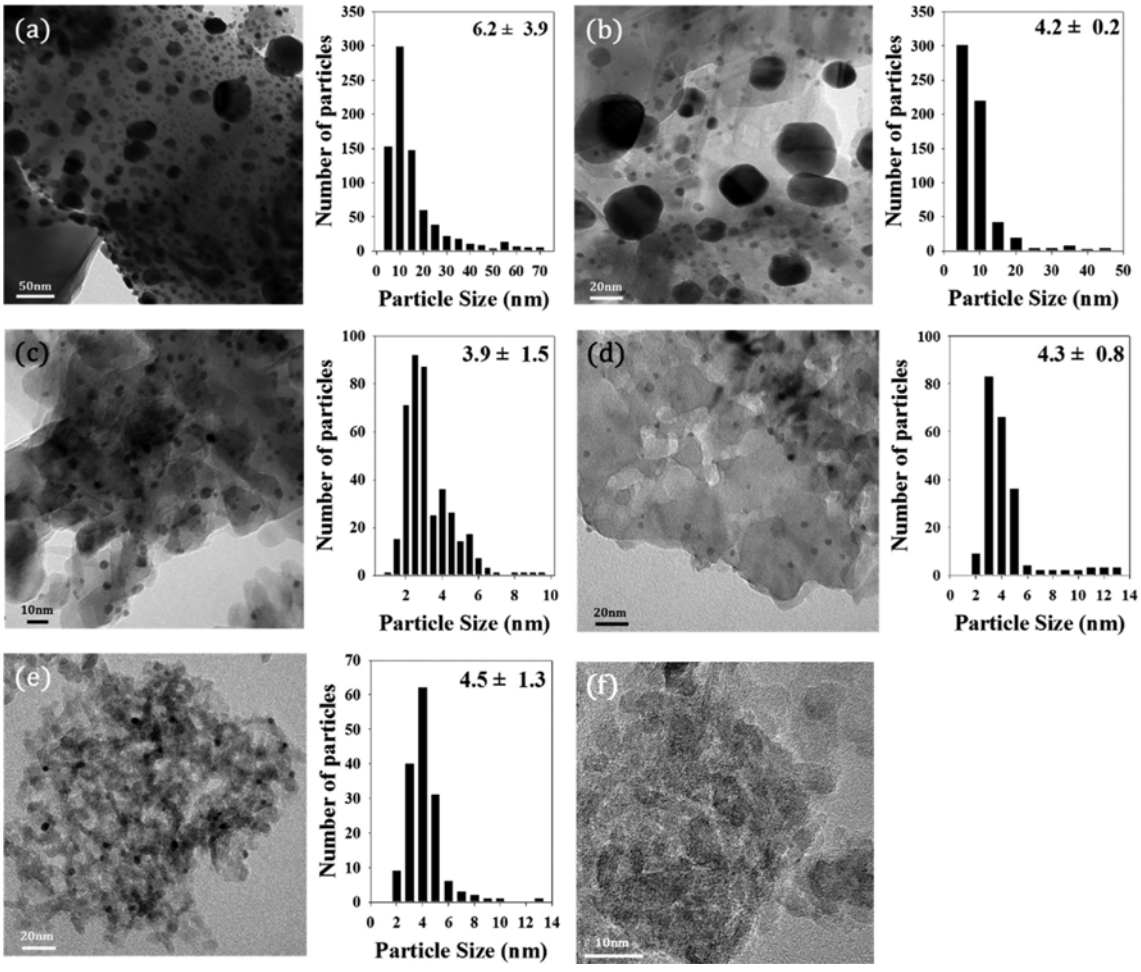

Fig. 3. TEM images and particle size distributions of Pt for Pt catalysts supported on different aluminum oxides: (a) Pt/α-Al_2O_3, (b) Pt/κ-Al_2O_3, (c) Pt/δ-Al_2O_3, (d) Pt/θ-Al_2O_3, (e) Pt/η-Al_2O_3, and (f) Pt/γ-Al_2O_3.

for Pt/α-Al_2O_3.

The Pt dispersion values of the Pt/Al_2O_3 catalysts were quantified based on the CO chemisorption data, as listed in Table 1. The calculations of the concentration of the exposed metallic Pt, as an active site, are based on the assumption that one CO molecule is adsorbed per Pt atom. The fraction of the surface Pt atoms per total Pt atoms, i.e., the so-called Pt dispersion, decreased in the following order: Pt/γ-Al_2O_3>Pt/δ-Al_2O_3>Pt/κ-Al_2O_3>Pt/θ-Al_2O_3>Pt/η-Al_2O_3>Pt/α-Al_2O_3.

TPO was carried out for all the supported Pt catalysts to investigate the oxygen-uptake behavior, as shown in Fig. 2. A very weak TPO peak was detected in the range 300-1,173 K for the Pt/α-Al_2O_3 catalyst, indicating that a very small amount of O_2 was continuously consumed with increasing temperature. For all catalysts, except for Pt/α-Al_2O_3, two separate TPO peaks were observed in the low- and high-temperature ranges. For these catalysts, a low-temperature TPO peak was detected in the range 300-850 K and a high-temperature TPO peak was observed in the range 850-1,173 K. The TPO peak areas correspond directly to the amount of O_2 consumed during the TPO experiments. The amount of O_2 consumed up to 850 K during the TPO experiments decreased in the following order: Pt/δ-Al_2O_3>Pt/η-Al_2O_3>Pt/θ-Al_2O_3>Pt/γ-Al_2O_3>Pt/κ-Al_2O_3>Pt/α-Al_2O_3.

The TEM image of the Pt/Al_2O_3 catalysts and the corresponding particle-size distribution of Pt particles are presented in Fig. 3. The size of the Pt particles in the Pt/Al_2O_3 catalysts is dependent on the support. Compared with Pt/α-Al_2O_3 and Pt/κ-Al_2O_3, where small Pt particles of less than 10 nm as well as agglomerates larger than 20 nm were observed, the other Pt catalysts were confirmed to have a rather narrow size distribution of Pt particles. The average Pt particle size for each Pt catalyst was calculated by counting Pt particles less than 10 nm and was determined to be 6.2±3.9, 4.2±0.2, 3.9±1.5, 4.3±0.8, and 4.5±1.3 nm for Pt/α-Al_2O_3, Pt/κ-Al_2O_3, Pt/δ-Al_2O_3, Pt/θ-Al_2O_3, and Pt/η-Al_2O_3, respectively. In the case of Pt/γ-Al_2O_3, the Pt particle size was estimated to be around 1 nm. This trend in the average particle size of Pt of the Pt catalysts is consistent with that of the calculated Pt particle size from CO chemisorption data.

FT-IR spectral analysis of the Pt/Al_2O_3 catalysts was performed after CO chemisorption to investigate the interaction between CO and the Pt species on each catalyst. As shown in Fig. 4, a very weak and broad peak with a maximum at 2,062 cm^{-1} was observed after CO chemisorption on Pt/α-Al_2O_3. A main peak at 2,064 cm^{-1} and a shoulder at 2,084 cm^{-1} were observed for Pt/κ-Al_2O_3, whereas

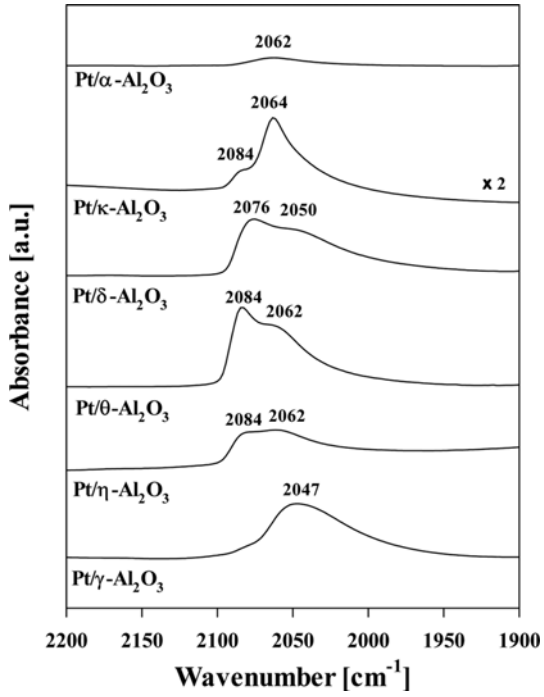

Fig. 4. IR spectra of Pt catalysts supported on different aluminum oxides after CO adsorption.

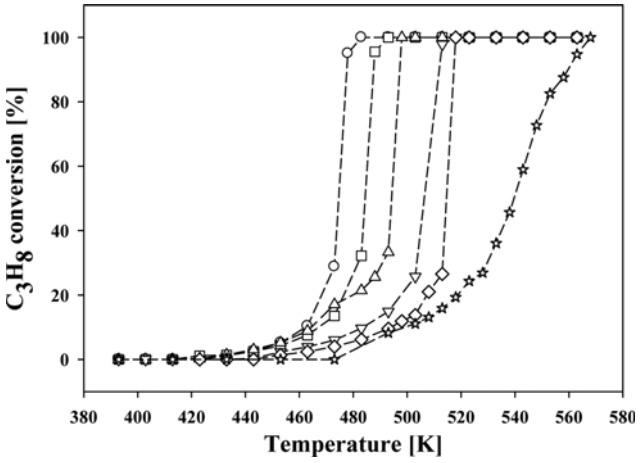

Fig. 5. Propane conversion with increasing reaction temperature over Pt catalysts supported on different aluminum oxides: Pt/α-Al_2O_3 (○), Pt/κ-Al_2O_3 (□), Pt/δ-Al_2O_3 (△), Pt/θ-Al_2O_3 (▽), Pt/η-Al_2O_3 (◇), and Pt/γ-Al_2O_3 (☆). F/W=1,000 mL/min/g_{cat}, feed composition: 1 mol% propane and 5 mol% O_2 in He.

the spectrum of Pt/δ-Al_2O_3 was characterized by a main peak at 2,076 cm^{-1} and a shoulder at 2,050 cm^{-1}. Pt/θ-Al_2O_3 and Pt/η-Al_2O_3 exhibited broad peaks with maxima at 2,084 and 2,062 cm^{-1}. In the case of Pt/γ-Al_2O_3, the CO band was observed at the lowest wavenumber, i.e., at 2,047 cm^{-1}. This band can be assigned to CO chemisorbed on well-dispersed Pt, which is associated with uncoordinated Pt sites, possibly at the edges or kinks between terraces or in extra-small particles consisting of only a few Pt atoms [29-31]. It has been reported that the CO IR band at low wavenumber (2,059-2,072 cm^{-1}) is due to CO that is linearly chemisorbed on highly dispersed Pt associated with high index planes [30]. On the other hand, the CO band at 2,085 cm^{-1} is attributed to CO linearly adsorbed on poorly dispersed Pt [31]. The CO-IR analysis clearly indicates that Pt particles with different sizes are present on the support, and that the Pt particle size is dependent on the support.

2. Performance of Pt/Al_2O_3 Catalysts in Propane Combustion

Fig. 5 shows the propane conversion achieved with the Pt catalysts supported on different types of alumina as a function of the reaction temperature. The rapid increase in the propane conversion with increasing reaction temperature, known as the ignition curve, is a typical phenomenon for this reaction. The propane-combustion activity of the catalysts decreased in the following order: Pt/α-Al_2O_3>Pt/κ-Al_2O_3>Pt/δ-Al_2O_3>Pt/θ-Al_2O_3>Pt/η-Al_2O_3>Pt/γ-Al_2O_3. Although the surface area and Pt dispersion were lowest for Pt/α-Al_2O_3, this catalyst showed the highest catalytic activity for propane combustion. On the other hand, the lowest catalytic activity for propane combustion was demonstrated by Pt/γ-Al_2O_3, which has the highest surface area and Pt dispersion. This result indicates that the larger Pt particles, which were prepared on supports with a low surface area, are more efficient catalysts for propane combustion than the smaller Pt particles, which were prepared on supports with a high surface area. The results are in agreement with those of a previous report stating that catalysts with small Pt particles exhibited low catalytic activity because of facile oxidation by O_2 [9].

The effect of the Pt particle size on the activity of the catalysts in propane combustion has been intensively investigated by several groups. Garetto et al. examined the effect of the size of Pt crystallites in a Pt/Al_2O_3 catalyst on its combustion activity, and suggested that propane combustion was a structure-insensitive reaction, as illustrated by the linear correlation between the Pt dispersion and catalytic activity [13]. Park et al. also reported that the specific reaction rate decreased with an increase in the Pt particle size in Pt/H-ZSM-5 [16]. In contrast, Yazawa et al. investigated the activity of Pt catalysts on various supports such as MgO, Al_2O_3, and SiO_2-Al_2O_3 for propane combustion and found that the turnover frequency (TOF) was inversely proportional to the Pt dispersion [8]. Independently, Beck et al. examined the catalytic activity for complete methane oxidation under lean conditions over size-controlled platinum nanoparticles supported on acid-pretreated γ-alumina and reported that the specific catalytic activity increased with increasing Pt particle size; the maximum TOF value was achieved for the catalysts containing partially oxidized platinum with a mean particle size of about 2 nm. The TOF decreased with further increase of the Pt particle size [32]. They attributed the strong size sensitivity to the size dependence of the apparent activation energy of the methane-oxidation and/or platinum-oxidation state in the catalytically active nanoparticles [32]. Overall, the effect of the Pt particle size on the activity of the catalysts for propane combustion is not straightforward. Other factors, including the support, promoter, poison, and reaction conditions may be interrelated, thereby affecting the oxidation state of Pt under working conditions, resulting in the variations of the catalytic activity with Pt particle size. It is generally accepted that metallic Pt is more active for complete oxida-

tion of CO and hydrocarbons than Pt oxide. Hicks et al. determined the intrinsic rates of methane oxidation in 5% excess oxygen over a series of platinum catalysts, and observed that the dispersed Pt was converted into PtO_2 while the crystallites were covered with adsorbed oxygen, and also found that the methane oxidation activity of dispersed PtO_2 is 10-100 times lower than that of platinum crystallites [33]. Weaver et al. demonstrated that Pt oxide particles were less active for CO oxidation than lower-coverage oxygen phases on Pt(111) and Pt(100), which was explained in terms of limited CO adsorption on the Pt oxide [34]. Gracia et al. observed that the TOF of CO oxidation increased with increasing particle size under O_2-rich conditions, confirming that the CO oxidation reaction over Pt/SiO_2 catalysts is structure-sensitive under an oxidizing environment [35]. They observed the formation of completely metallic Pt particles upon reduction in H_2 at 573 K for 1 h regardless of the particle size. However, with subsequent oxidation treatment, only the smallest particles were fully oxidized [35]. They reported that metallic Pt is the active surface of the Pt/SiO_2 catalysts for CO oxidation, and that different sites on the Pt crystallite lead to different oxidation rates depending on the size [35]. In this study, aluminum oxides with different crystalline structures were utilized as supports for Pt catalysts without any promoter. Based on the TPO data, it is proposed that Pt metal can be oxidized by oxygen in the feed stream below the temperature where propane combustion occurs (Fig. 5). Therefore, high catalytic activity can be achieved with Pt catalysts having large Pt particles that are resistant to Pt oxidation.

To determine the apparent activation energy for this reaction over the respective catalysts, the specific reaction rate was determined at different temperatures for the reaction over each catalyst under differential reactor conditions. The Arrhenius plot, in which the rate of propane combustion is plotted at different reaction temperatures, was obtained for each catalyst as shown in Fig. 6. The specific reaction rate for propane combustion decreased in the following order: $Pt/\alpha\text{-}Al_2O_3$>$Pt/\kappa\text{-}Al_2O_3$>$Pt/\delta\text{-}Al_2O_3$>$Pt/\theta\text{-}Al_2O_3$>$Pt/\eta\text{-}Al_2O_3$>$Pt/\gamma\text{-}Al_2O_3$. The apparent activation energies for $Pt/\alpha\text{-}Al_2O_3$, $Pt/\kappa\text{-}Al_2O_3$, $Pt/\delta\text{-}Al_2O_3$, $Pt/\theta\text{-}Al_2O_3$, $Pt/\eta\text{-}Al_2O_3$, and $Pt/\gamma\text{-}Al_2O_3$ were determined to be 24.7, 21.4, 24.3, 22.1, 24.0, and 19.1 kcal/mol, respectively. Notably, the apparent activation energy was similar for all the catalysts, except for $Pt/\gamma\text{-}Al_2O_3$ with slightly lower apparent activation energy. The apparent activation energy in this study is similar to that (22.1±3.4 kcal/mol) determined using 0.03-30 wt% of Pt/Al_2O_3 catalysts [36] and is slightly higher than that (17.0 kcal/mol) determined using 0.33% Pt/Al_2O_3 [13].

The thermal stability of the supported Pt catalyst was evaluated based on cyclic tests carried out using $Pt/\alpha\text{-}Al_2O_3$ and $Pt/\delta\text{-}Al_2O_3$. The catalytic activity of the used catalyst after treatment at 773 K under similar reaction conditions was compared with that of the fresh catalyst. In the case of $Pt/\alpha\text{-}Al_2O_3$, no noticeable change in the catalytic activity was observed during the cyclic test (data not shown). On the other hand, the catalytic activity of $Pt/\delta\text{-}Al_2O_3$ increased with increasing numbers of cycles in the test, as shown in Fig. 7. The shift of the propane conversion curves toward lower temperature clearly indicates that the catalytic activity of the thermally-treated catalyst is enhanced relative to that of the fresh catalyst. Given that the catalyst was reduced with hydrogen at 673 K prior to each cyclic test, no change in the oxidation state of Pt is expected. To determine if the Pt particle size changed during the cyclic test, the TEM image of the spent $Pt/\delta\text{-}Al_2O_3$ catalyst was obtained, as shown in Fig. 8. The average Pt particle size was determined to be 4.5±3.3 for the spent $Pt/\delta\text{-}Al_2O_3$, which was larger than that (3.9±1.5) of the fresh counterpart. This also clearly confirms that larger Pt particles are favorable for propane combustion. In this case, the only effect of Pt particle size on the catalytic activity

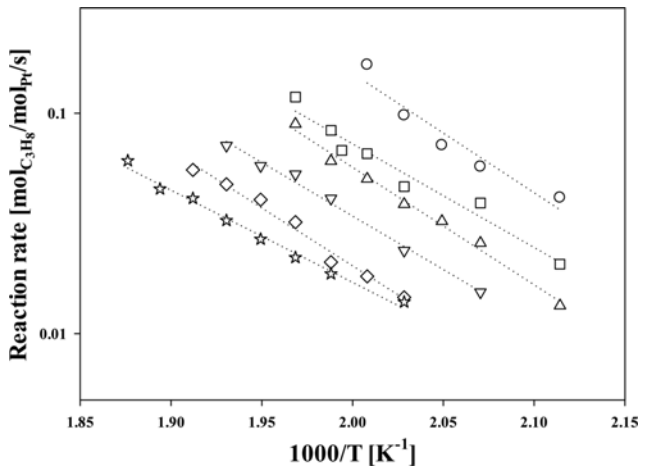

Fig. 6. Reaction rate as a function of temperature for propane combustion over Pt catalysts supported on different aluminum oxides: $Pt/\alpha\text{-}Al_2O_3$ (○), $Pt/\kappa\text{-}Al_2O_3$ (□), $Pt/\delta\text{-}Al_2O_3$ (△), $Pt/\theta\text{-}Al_2O_3$ (▽), $Pt/\eta\text{-}Al_2O_3$ (◇), and $Pt/\gamma\text{-}Al_2O_3$ (☆). Feed composition: 1 mol% propane and 5 mol% O_2 in He.

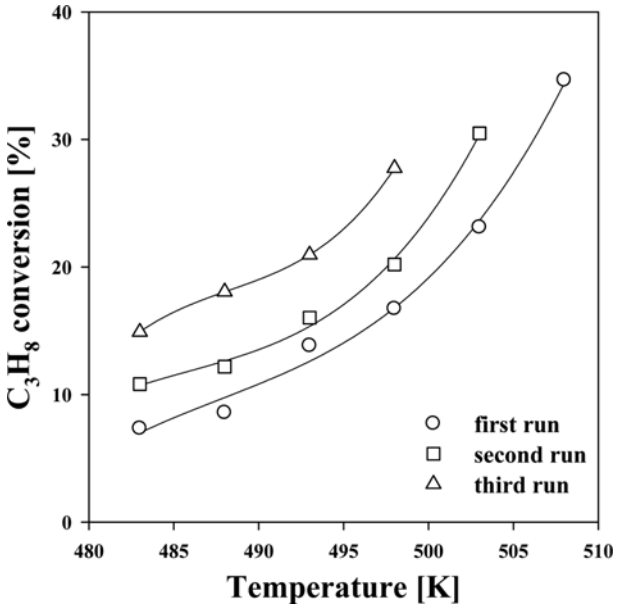

Fig. 7. Temperature dependence of propane conversion over $Pt/\delta\text{-}Al_2O_3$ catalyst after the first (□) and second (△) thermal treatments. F/W=2,500 mL/min/g_{cat}, feed composition: 1 mol% propane and 5 mol% O_2 in He. The thermal treatment was carried out at 773 K for 1 h using the same feed composition. The catalyst was reduced with H_2 at 673 K before each activity test.

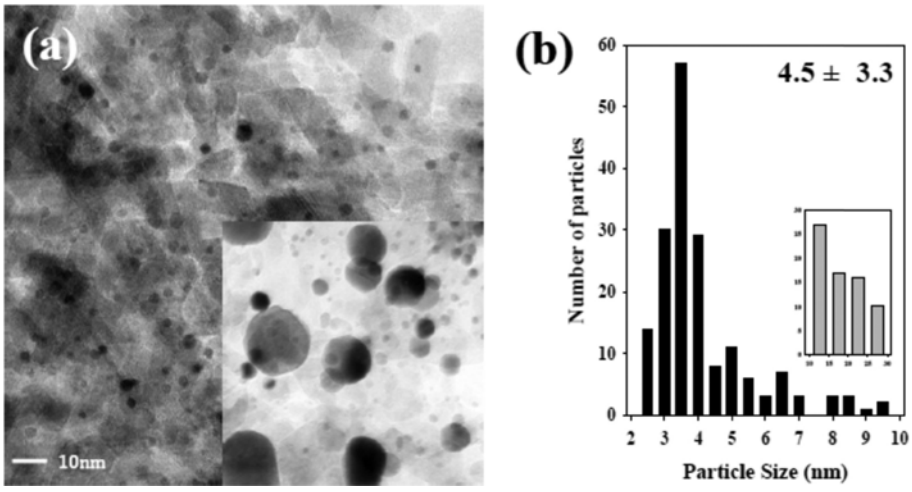

Fig. 8. TEM image (a) and particle size distribution of Pt (b) of the Pt/δ-Al_2O_3 catalyst after cyclic test. The reaction conditions were identical to those in Fig. 7.

for propane combustion could be evaluated. Now, we can conclude that the propane combustion is a structure-sensitive reaction.

For propane combustion over supported Pt catalysts, the crystallite size and oxidation state of Pt are critical factors affecting the catalytic activity and these factors are closely interrelated given that the oxidation state of Pt is strongly dependent on the Pt particle size in lean conditions (i.e., oxygen-rich conditions) [35]. These key factors are influenced by the physicochemical properties (i.e., surface area, surface acidity, surface defects, and oxygen mobility) of the support, promoter, and reaction conditions. A large surface area of the support is beneficial for achieving a high Pt dispersion. The surface acidity of the support might contribute to stabilization of metallic Pt [7,8]. The Pt dispersion and its oxidation state are also affected by the promoter. The data in this study confirmed that the Pt dispersion is one of important factors for determining the activity of Pt/Al_2O_3 catalysts, and a low Pt dispersion, which might be related to the oxidation resistance of Pt, is advantageous for this reaction. A similar observation was reported for the selective CO oxidation in the presence of hydrogen over supported Ru catalyst [37].

CONCLUSIONS

Pt catalysts supported on various aluminum oxides (α-Al_2O_3, κ-Al_2O_3, δ-Al_2O_3, θ-Al_2O_3, η-Al_2O_3, and γ-Al_2O_3) were applied to propane combustion. Although Pt dispersion is not directly related to the BET surface area of the catalyst support, the lowest and highest Pt dispersions were respectively achieved for Pt/α-Al_2O_3 and Pt/γ-Al_2O_3, which has the smallest and largest BET surface areas, respectively. Among the evaluated Pt/Al_2O_3 catalysts, Pt/α-Al_2O_3 catalysts with the lowest Pt dispersion and surface area showed the highest propane combustion activity. In contrast, Pt/γ-Al_2O_3 catalysts with the highest Pt dispersion and surface area were characterized by the lowest propane combustion activity. The presence of large Pt particles on α-Al_2O_3 with a low surface area was associated with enhanced resistance toward Pt oxidation, confirmed by TPO analysis, resulting in high catalytic activity for propane combustion.

ACKNOWLEDGEMENT

This research was supported by the Basic Science Research Program through the National Research Foundation of Korea (NRF), funded by the Ministry of Education (NRF-2009-0094046) and the New & Renewable Energy grant of the Korea Institute of Energy Technology Evaluation and Planning (20123010040010) funded by the Korea Government Ministry of Knowledge Economy. This work was also supported by an Ajou University Research Fellowship, 2012 (S-2012-G0001-00067).

REFERENCES

1. T. V. Choudhary, S. Banerjee and V. R. Choudhary, *Appl. Catal. A: Gen.*, **234**, 1 (2002).
2. Y.-F. Yu Yao, *Ind. Eng. Chem. Prod. Res. Dev.*, **19**, 293 (1980).
3. K. B. Kim, M. K. Kim, Y. H. Kim, K. S. Song and E. D. Park, *Res. Chem. Intermed.*, **36**, 603 (2010).
4. J. Okal and M. Zawadzki, *Appl. Catal. B: Environ.*, **105**, 182 (2011).
5. L. Kiwi-Minsker, I. Yuranov, E. Slavinskaia, V. Zaikovski and A. Renken, *Catal. Today,* **59**, 61 (2000).
6. Y. Men, G. Kolb, R. Zapf, H. Pennemann and V. Hessel, *Chem. Eng. Res. Des.*, **87**, 91 (2009).
7. Y. Yazawa, N. Takagi, H. Yoshida, S.-I. Komai, A. Satsuma, T. Tanaka, S. Yoshida and T. Hattori, *Appl. Catal. A: Gen.*, **233**, 103 (2002).
8. Y. Yazawa, H. Yoshida and T. Hattori, *Appl. Catal. A: Gen.*, **237**, 139 (2002).
9. J. E. Park, K. B. Kim, K. W. Seo, K. S. Song and E. D. Park, *Res. Chem. Intermed.*, **37**, 1135 (2011).
10. M. S. Avila, C. I. Vignatti, C. R. Apesteguia and T. F. Garetto, *Chem. Eng. J.*, **241**, 52 (2014).
11. C. P. Hubbard, K. Otto, H. S. Gandhi and K. Y. Ng, *J. Catal.*, **144**, 484 (1993).
12. R. Burch, E. Halpin, M. Hayes, K. Ruth and J. A. Sullivan, *Appl. Catal. B: Environ.*, **19**, 199 (1998).

13. T. F. Garetto, E. Rincon and C. R. Apesteguia, *Appl. Catal. B: Environ.*, **48**, 167 (2004).
14. T. F. Garetto, E. Rincón and C. R. Apesteguía, *Appl. Catal. B: Environ.*, **73**, 65 (2007).
15. K. B. Kim, Y. H. Kim, K. S. Song and E. D. Park, *Rev. Adv. Mater. Sci.*, **28**, 35 (2011).
16. J. E. Park, K. B. Kim, Y.-A. Kim, K. S. Song and E. D. Park, *Catal. Lett.*, **143**, 1132 (2013).
17. H. Yoshida, Y. Yazawa and T. Hattori, *Catal. Today,* **87**, 19 (2003).
18. Y. Yazawa, H. Yoshida, S.-I. Komai and T. Hattori, *Appl. Catal. A: Gen.*, **233**, 113 (2002).
19. M. S. Avila, C. I. Vignatti, C. R. Apesteguia, V. V. Rao, K. Chary and T. F. Garetto, *Catal. Lett.*, **134**, 118 (2010).
20. M.-Y. Kim, S. M. Park, G. Seo and K.-S. Song, *Catal. Lett.*, **137**, 205 (2010).
21. M. J. Tiernan and O. E. Finlayson, *Appl. Catal. B: Environ.*, **19**, 23 (1998).
22. Z. Zhu, G. Lu, Y. Guo, Y. Guo, Z. Zhang, Y. Wang and Z.-Q. Gong, *ChemCatChem,* **5**, 2495 (2013).
23. W. Xiaodong, Z. Li, W. Duan, L. Shuang, S. Zhichun and F. Jun, *J. Hazard. Mater.*, **225-226**, 146 (2012).
24. Y. H. Kim and E. D. Park, *Appl. Catal. B: Environ.*, **96**, 41 (2010).
25. S. Rane, Ø. Borg, J. Yang, E. Rytter and A. Holmen, *Appl. Catal. A: Gen.*, **388**, 160 (2010).
26. R. Burch and P. K. Loader, *Appl. Catal. B: Environ.*, **5**, 149 (1994).
27. G. Bergeret and P. Gallezot, in *Handbook of Heterogeneous Catalysis*, G. Ertl, H. Knözinger, F. Schüth and J. Weitkamp Eds., Wiley-VCH, Weinheim (2008).
28. C.-P. Hwang and C.-T. Yeh, *J. Mol. Catal. A: Chem.*, **112**, 295 (1996).
29. S. Thomas, M. Rivallan, M. Lepage, N. Takagi, H. Hirata and F. Thibault-Starzyk, *Micropor. Mesopor. Mater.*, **140**, 103 (2011).
30. J. A. Anderson, F. K. Chong and C. H. Rochester, *J. Mol. Catal. A: Chem.*, **140**, 65 (1999).
31. D. Liu, G.-H. Que, Z.-H. Wang and Z.-F. Yan, *Catal. Today,* **68**, 155 (2001).
32. I. E. Beck, V. I. Bukhtiyarov, I. Y. Pakharukov, V. I. Zaikovsky, V. V. Kriventsov and V. N. Parmon, *J. Catal.*, **268**, 60 (2009).
33. R. F. Hicks, H. Qi, M. L. Young and R. G. Lee, *J. Catal.*, **122**, 280 (1990).
34. J. F. Weaver, H. H. Kan and R. B. Shumbera, *J. Phys.: Condens. Matter,* **20**, 184015 (2008).
35. F. J. Gracia, L. Bollmann, E. E. Wolf, J. T. Miller and A. J. Kropf, *J. Catal.*, **220**, 382 (2003).
36. K. Otto, J. W. Andino and C. L. Parks, *J. Catal.*, **131**, 243 (1991).
37. J. E. Park and E. D. Park, *Korean J. Chem. Eng.*, **31**(11), 1985 (2014).